

Corrosion Characteristics of Hydrotalcite and Mg(OH)₂ Surfaces of AZ31 Alloy Accomplished via Hydrothermal Surface Modification

A. DHANALAKSHMI^{1,2} and A. CYRIL^{2,*}

¹Department of Chemistry, Alagappa University, Karaikudi-630003, India

²Post Graduate and Research Department of Chemistry, Raja Doraisingam Government Arts College, Sivaganga-630561, India

*Corresponding author: E-mail: cyrilchemistry03@gmail.com

Received: 17 February 2019;

Accepted: 29 March 2019;

Published online: 21 May 2019;

AJC-19419

In this work, the surface of AZ31-Mg alloy is modified by hydrothermal treatment in high alkali solutions to attain high corrosion resistance. A class of magnesium hydroxide family with a layer structured compound hydrotalcite [Mg₆Al₂CO₃(OH)₁₆·4H₂O] rhombohedral phase has been formed along with hexagonal Mg(OH)₂ phases on AZ31 alloy surface. The hydrotalcite and hexagonal Mg(OH)₂ phases were confirmed by X-ray diffraction analysis. The modified surfaces of AZ31 alloy are examined by field emission scanning electron microscope and location specific elemental compositions are obtained by EDS analysis. The hydrotalcite and Mg(OH)₂ corrosion behavior was analyzed in 3.5 % NaCl electrolyte. For comparison purpose, only hexagonal Mg(OH)₂ surfaces were also prepared by hydrothermal treatment and compared the corrosion rates with the hydrotalcite surfaces. The linear polarization and electrochemical impedance spectroscopy results revealed that the hydrotalcite surfaces demonstrated more noble or positive shift on open circuit potential, corrosion current density and resistance than those of only hexagonal Mg(OH)₂ and bare AZ31 alloy. The formation of layered double hydroxide of magnesium with carbonates on AZ31 alloy led the more protection and this work paves newer directions on hydrothermal surface modification of Mg alloys.

Keywords: Corrosion, AZ31, Magnesium alloy, Mg(OH)₂, Hydrotalcite.

INTRODUCTION

Low density and high strength magnesium alloys have attracted more attention in the research and development due to their applications as structural metallic materials in aerospace and automotive and biomedical applications [1-4]. The high strength and weight ratio of magnesium alloys opens wide applications and found to be a candidate material to replace steel and aluminum alloys. However, in practical applications, magnesium alloys are not standing as strong competent to others due to the poor corrosion resistance, which is a main disadvantage. The high chemical reactivity, magnesium alloys exhibits higher corrosion rates even in atmospheric and other mediums of corrosion tests [5-12]. Two types of approaches were employed on Mg alloys to improve corrosion resistance; one is alloying [13] and the second is application of external coatings. The addition of Al, Zn, Mn and rare-earth elements improves the corrosion resistance of magnesium alloys. The external coatings developed by various methods such as plating and anodizing

[14,15], chemical conversion coatings [16], sol-gel coatings and laser surface treatments [17,18], chemical and physical vapour deposition techniques [19-21] and thermal spray coatings [22], where the corrosion resistance can be greatly improved because it is entirely determined by the property of the materials covering magnesium alloys. Among the various coatings materials, hexagonal Mg(OH)₂ demonstrated excellent corrosion resistance and used as flame retardant [23], catalyst [24], carbon dioxide absorbent [25], which can be synthesized into various shapes like nano-flower, nano-plates, nano-rod and tubes by electro-deposition and hydrothermal approaches [26-29].

The AZ31 alloy is used as magnesium alloy in the present study magnesium alloy AZ31 (composition: 2.98 % Al; 0.88 % Zn; 0.38 % Mn; 0.0135 % Si; 0.001 % Cu; 0.002 % Ni; 0.0027 % Fe and the rest is Mg). The hexagonal Mg(OH)₂ protective films were developed hydrothermal treatment in the previous works [30-32]. Ishizaki *et al.* [32] fabricated vertically aligned Mg_{1-x}Al_x(OH)₂(NO₃)_x·nH₂O, Mg_{1-x}Al_x(OH)₂(NO₃)_x·nH₂O and Mg(OH)₂ and Mg(OH)₂ nano-sheets on a magnesium alloy

substrate (AZ31), however the corrosion behavior of layered double hydroxides has not been investigated. Zhu *et al.* [31] demonstrated that $\text{Mg}_2\text{Al}(\text{OH})_7$ phase show additional benefits in terms of corrosion resistance along with $\text{Mg}(\text{OH})_2$ prepared *via* hydrothermal treatment.

In this work, layered double hydroxide carbonate, hydroxalcalite [$\text{Mg}_6\text{Al}_2\text{CO}_3(\text{OH})_{16}\cdot 4\text{H}_2\text{O}$] rhombohedral phase has been formed along with hexagonal $\text{Mg}(\text{OH})_2$ phases on AZ31 alloy surface *via* hydrothermal treatment. Hydroxalcalite is layered double hydroxide where divalent cations replaced by trivalent cations and is a synthetic compound which is broadly investigated due to its potential applications in high temperature porous insulating ceramics, catalysts, adsorptive flotation. Nevertheless, the corrosion protection properties of hydroxalcalite mixed with hexagonal magnesium hydroxide films, which are grown *via* hydrothermal treatment, are not studied till now. Hence, the current study deals on the fabrication of hydroxalcalite and $\text{Mg}(\text{OH})_2$ mixed film on AZ31 alloy *via* hydrothermal method and corrosion characteristics were investigated. The linear polarization and electrochemical impedance spectroscopy results revealed that the hydroxalcalite surfaces demonstrated more noble or positive shift on open circuit potential, corrosion current density and resistance than those of only hexagonal $\text{Mg}(\text{OH})_2$ and bare AZ31 alloy.

EXPERIMENTAL

Sample preparation: The sample with 11 mm × 11 mm × 8 mm dimensions were cut from sheet and polished from 200 to 1200 SiC grit paper and mirror polished using 0.5 μm diamond paste embedded cloth using metallurgical polishing machine.

Fabrication of $\text{Mg}(\text{OH})_2$ surface by hydrothermal method: First, 5.5 % NaOH is dissolved in 30 mL of deionized water and stirred for 10 min. Then the solution transferred to 50 mL Teflon lined stainless steel autoclave. To this, the cut and polished and washed specimen of AZ31 was placed in the solution, which was in autoclave and kept in 170 °C for 8 h period. Then the autoclave was cooled to room temperature and the sample was removed and washed with running distilled water several times and dried in vacuum oven.

Similarly, for fabricating layered double hydroxide carbonates hydroxalcalite mixed with hexagonal $\text{Mg}(\text{OH})_2$ films on AZ31 alloy, SrCl_2 (0.5 mol) was dissolved in deionized water and high molar NaOH solution was added dropwise under continuous stirring. After a white colour precipitate formed, the solution of 30 mL was transferred to 50 mL of Teflon lined stainless steel autoclave. To this, the polished sample of AZ31 was immersed in the solution and kept in 170 °C for the period of 8 h. Then the sample removed from the cooled autoclave the white colour precipitate and samples were separated. The samples were washed several times to remove the impurities.

Characterization: The surface of the samples are examined by X-ray diffraction analysis (XRD), surface morphologies and elemental analysis by field emission scanning electron microscopy (FESEM) and energy dispersive spectroscopy (EDS) analysis. The samples were then soldered with copper wire for electrochemical analysis. After corrosion, the surfaces of the samples were also examined by XRD and FESEM and EDS analysis.

Electrochemical experiments: A three electrode system was used for analyzing the open circuit potentials. Tafel plots was used to determine the corrosion current densities and electrochemical impedance spectroscopy. The AZ31 specimens as working electrode, saturated calomel (SCE) as reference electrode and platinum foil as counter electrode were employed. The electrolytes of 3.5 % NaCl and 5 % $(\text{NH}_4)_2\text{CO}_3$ were used in the present work.

RESULTS AND DISCUSSION

X-ray diffraction analysis: The XRD patterns of bare AZ31 alloy, hydrothermal modified surfaces of $\text{Mg}(\text{OH})_2$ and hydroxalcalite [$\text{Mg}_6\text{Al}_2\text{CO}_3(\text{OH})_{16}\cdot 4\text{H}_2\text{O}$] are shown in Fig. 1. The bare AZ31 alloy exhibits sharp peaks, which are well matched to standard JCPDS file no. # 35-0821. The peaks and the corresponding planes indicate that the hexagonal crystal structure with a space group of $P6_3/mmc$ for Mg alloy. The crystal lattice parameters are $a = b = 3.2094 \text{ \AA}$ and $c = 5.211 \text{ \AA}$.

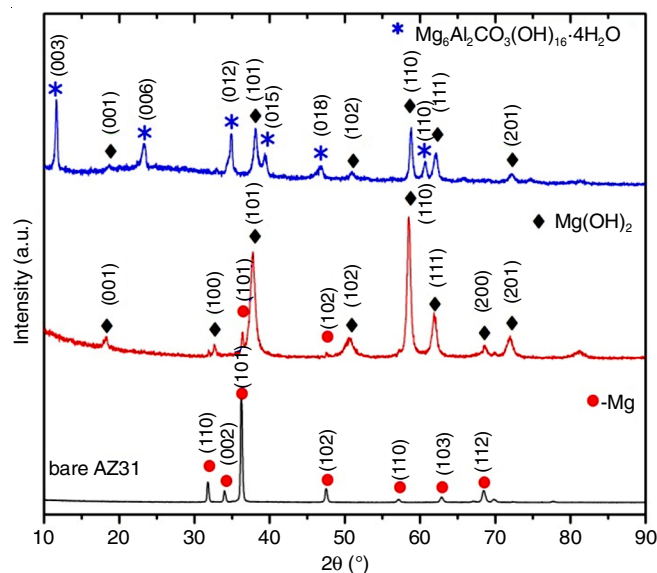


Fig. 1. XRD patterns of of bare AZ31 alloy, hydrothermal modified surfaces of $\text{Mg}(\text{OH})_2$ and hydroxalcalite [$\text{Mg}_6\text{Al}_2\text{CO}_3(\text{OH})_{16}\cdot 4\text{H}_2\text{O}$]

Similarly, XRD pattern for the surface with $\text{Mg}(\text{OH})_2$ film indicate high crystalline peaks and all the peaks are well matched with standard JCPDS file no. # 07-0239. The indexed peaks show that the hexagonal crystal structure for $\text{Mg}(\text{OH})_2$ films, which is also called as brucite. The hexagonal $\text{Mg}(\text{OH})_2$ belongs to $P-3m1$ space group with the lattice parameters of $a = b = 3.147 \text{ \AA}$ and $c = 4.769 \text{ \AA}$. The changes in lattice parameters clearly indicate the surface modification of AZ31 Mg alloy. Similar XRD patterns also observed in the literature works on $\text{Mg}(\text{OH})_2$ surfaces [30-32].

Further, XRD pattern for the surface with carbonate film demonstrates high crystalline peaks, which are well matched with standard JCPDS file no. # 70-2151. The indexed peaks showed that rhombohedral crystal structure for hydroxalcalite ($\text{Mg}_6\text{Al}_2\text{CO}_3(\text{OH})_{16}\cdot 4\text{H}_2\text{O}$) films, which is also called as hydroxalcalite. The rhombohedral hydroxalcalite ($\text{Mg}_6\text{Al}_2\text{CO}_3(\text{OH})_{16}\cdot 4\text{H}_2\text{O}$) films belongs to $R-3m$ space group with the lattice parameters of $a = b = 3.057 \text{ \AA}$ and $c = 22.81 \text{ \AA}$. The peaks are also well

matched with literatures [33,34]. The optimum ratio for hydrotalcite formation found to be 69 wt. % $\text{Mg}(\text{OH})_2$ /31 wt% $\text{Al}(\text{OH})_3$.

Raman spectroscopy: The laser Raman spectra of bare AZ31 alloy, bare AZ31 alloy, hydrothermal modified surfaces of $\text{Mg}(\text{OH})_2$ and hydrotalcite [$\text{Mg}_6\text{Al}_2\text{CO}_3(\text{OH})_{16}\cdot 4\text{H}_2\text{O}$] are presented in Fig. 2. The magnesium is silent for Raman, for detecting the carbonate and hydroxide peaks.

Fig. 2a represents the laser Raman spectrum for bare AZ31 alloy demonstrate two major peaks at 500 and 3600 cm^{-1} wave number, which corresponds to metal carbonate and hydroxyl peaks, respectively. Fig. 2b shows the Raman spectrum for surfaces of $\text{Mg}(\text{OH})_2$ and Fig. 2c shows the hydrotalcite [$\text{Mg}_6\text{Al}_2\text{CO}_3(\text{OH})_{16}\cdot 4\text{H}_2\text{O}$]. The intensities of both carbonate and hydroxyl peaks found very meager for bare alloy, indicating small or trace amount of magnesium carbonate and magnesium hydroxide films formed on bare alloy. However, the peaks of both magnesium carbonate and magnesium hydroxide found to increase for $\text{Mg}(\text{OH})_2$ and even more for hydrotalcite surfaces.

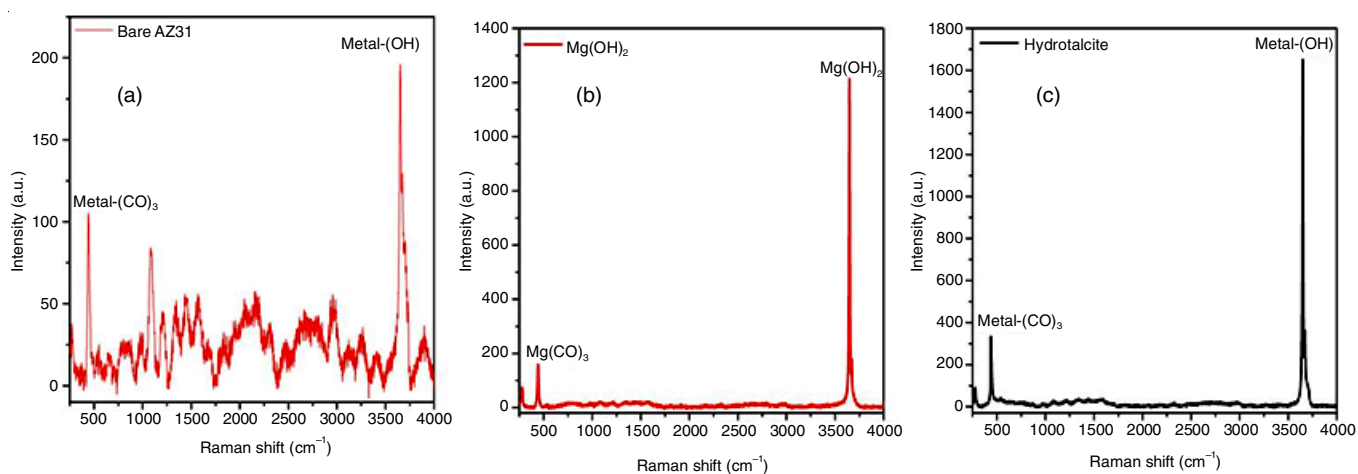


Fig. 2. Laser Raman spectra of bare AZ31 alloy, of bare AZ31 alloy, hydrothermal modified surfaces of $\text{Mg}(\text{OH})_2$ and hydrotalcite [$\text{Mg}_6\text{Al}_2\text{CO}_3(\text{OH})_{16}\cdot 4\text{H}_2\text{O}$]

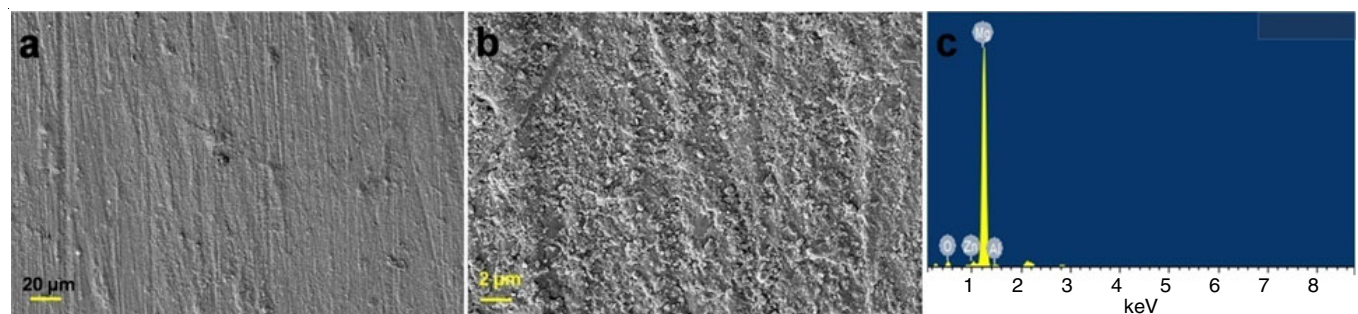


Fig. 3. Lower and higher magnified surface morphological features of bare AZ31 and elemental EDS spectrum

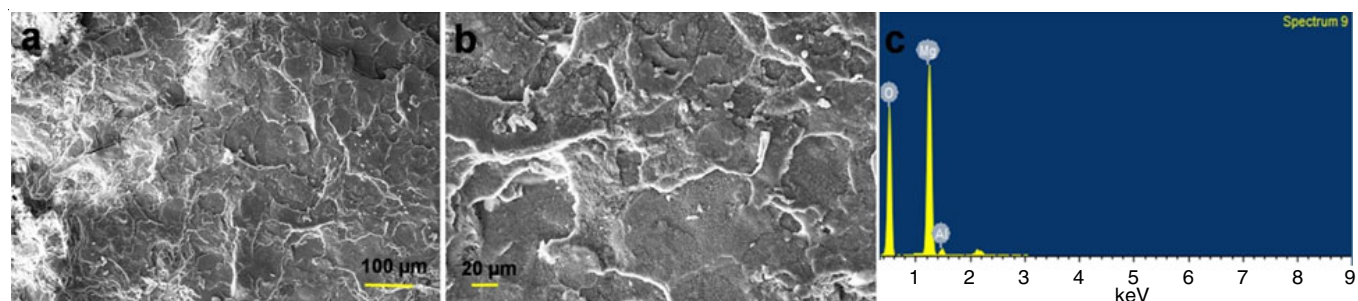


Fig. 4. Lower and higher magnified surface morphological features of $\text{Mg}(\text{OH})_2$ films and elemental EDS spectrum

This indicates that the protective film hydrotalcite formed on the surface of magnesium alloy during the hydrothermal treatment.

Surface morphology: The surface morphological images of bare AZ31 are shown in Fig. 3. Fig. 3a is a lower magnified image of AZ31 without any surface treatment while Fig. 3b shows the higher magnified images of AZ31 and the corresponding EDS spectrum is shown in Fig. 3c. The EDS profile demonstrates the presence of Mg, Al and Zn as major elements with trace amounts of oxygen, which is not avoidable due to surface reactivity of bare magnesium alloy in atmosphere.

Similarly, the surface morphological feature of $\text{Mg}(\text{OH})_2$ films are shown in Fig. 4. The lower and higher magnified images show the different morphology in comparison with bare AZ31. A layered structure is seen on the hydrothermally modified surface. The EDS analysis shows Mg as major and Al as minor elements along with predominant signal corresponds to oxygen. These observations clearly indicate the Mg-OH surface. The

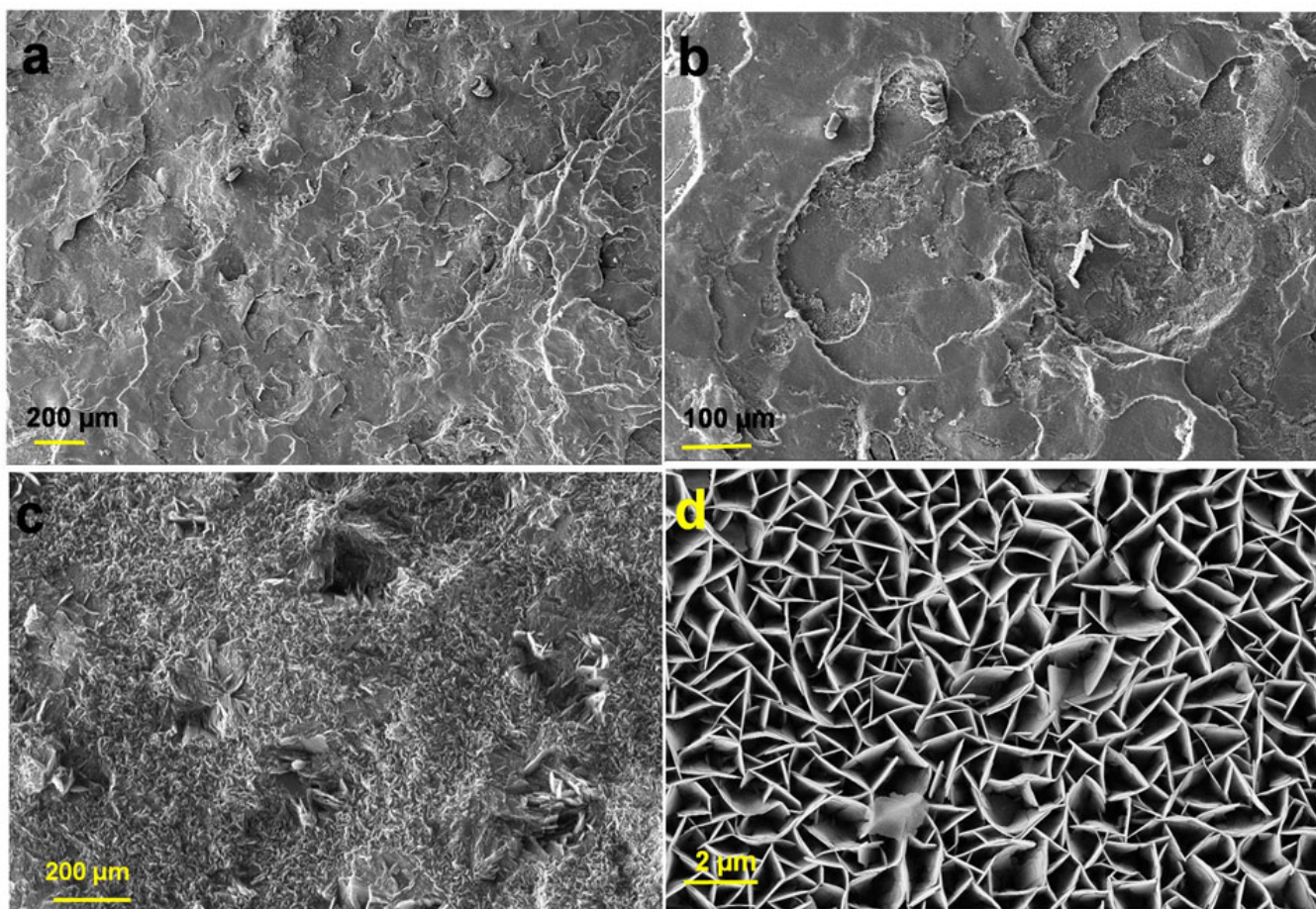
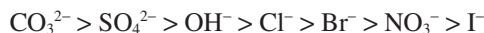


Fig. 5. Surface morphological images of hydrotalcite films $[\text{Mg}_6\text{Al}_2\text{CO}_3(\text{OH})_{16}\cdot 4\text{H}_2\text{O}]$

element Zn is not identified after hydrothermal treatment due to the formation of thick $\text{Mg}(\text{OH})_2$ film on AZ31 alloy.

Further, the surface morphology of hydrotalcite is analyzed through SEM and the corresponding images are presented in Fig. 5. Fig. 5a-d are the lower and higher magnification surface morphological images of hydrotalcite films developed *via* hydrothermal treatment.

Though the surface morphologies at lower magnifications exhibit similar to $\text{Mg}(\text{OH})_2$ surface, however the higher magnification image demonstrate clear distinct-flake type morphology. The preferential crystal growth in lower atomic adsorption energy crystallographic planes as noticed in previous works [35-37]. These observations demonstrates the dissolution/hydration and co-precipitation mechanism for MgO and $\text{Al}(\text{OH})_3$. The charge imbalance develops between the sheets and destructs the interlamellar hydrogen bonds in the crystallites of oxide-hydroxides. Further, the intercalation of CO_3^{2-} and balances the charge balance. Ostwald ripening is the main crystal growth mechanism and the aspect ratio of plates decreases with an increase in alkali concentration [38-41]. The preference of hydrotalcite with different anions is shown below as [42]:



Electrochemical analysis: The potentiodynamic polarization curves of bare AZ31, $\text{Mg}(\text{OH})_2$ and hydrotalcite in 3.5 % NaCl electrolyte are shown in Fig. 6. Electrochemical impedance behaviour of these samples in the same electrolyte is shown in Fig. 7. The Tafel plots demonstrates the corrosion

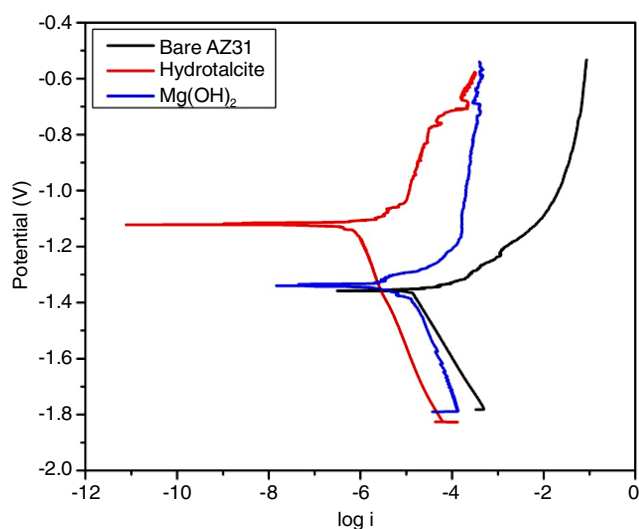


Fig. 6. Potentiodynamic polarization curves and electrochemical impedance behaviour of bare AZ31, $\text{Mg}(\text{OH})_2$ and hydrotalcite $[\text{Mg}_6\text{Al}_2\text{CO}_3(\text{OH})_{16}\cdot 4\text{H}_2\text{O}]$ in 3.5 NaCl electrolyte

potentials (E_{corr}) and corrosion current densities of AZ31 alloy and hydrothermally treated surfaces of $\text{Mg}(\text{OH})_2$ and hydrotalcite. From Fig. 6, it is noted that the corrosion potential of bare AZ31 found to be -1.4 V; for $\text{Mg}(\text{OH})_2$ is -1.37 V and for hydrotalcite surface found to be -1.16 V. The hydrotalcite surface demonstrate more positive potentials than $\text{Mg}(\text{OH})_2$ and bare AZ31 alloys indicating more protective nature of surface film.

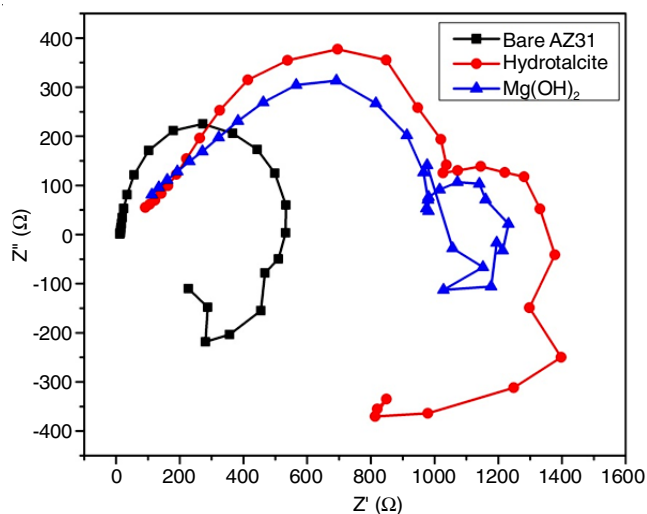


Fig. 7. Electrochemical impedance behaviour of bare AZ31, Mg(OH)₂ and hydrotalcite [Mg₆Al₂CO₃(OH)₁₆·4H₂O] in 3.5 NaCl electrolyte

The corrosion current densities found to be 7.21×10^{-5} , 3.1×10^{-6} and 4.2×10^{-7} A/cm² for bare AZ31, Mg(OH)₂ and hydrotalcite, respectively. The I_{corr} value found to be lower for hydrotalcite surface, which indicate the lower corrosion rates and higher protection properties than those of others. Electrochemical impedance spectroscopic analysis was further conducted in 3.5 % NaCl to study the stability of films. All the Nyquist plots were composed of capacitive and inductive arcs, where the capacitive arc associates with the charge transfer resistance. The larger diameter denotes higher corrosion resistance [43,44]. Fig. 7 shows two capacitive arcs for surface treated alloy, while bare AZ31 shows only one. Two capacitive arcs are more common in coated surfaces or films due to the high or low frequencies related to the substrate/coating [45]. The equivalent circuit of $R_s(C_{dl}R_t(R_LL))$ was used fit the Nyquist plot of bare AZ31 curve, while $R_s(C_f(R_p(C_{dl}R_t(R_LL))))$ was used for Mg(OH)₂ and hydrotalcite films, which have two conductive loops. In those, R_p and C_f represent pore resistance and capacitance of films, C_{dl} and R_t represent the double layer capacitance and the charge transfer resistance of the substrate, R_L and L represent the inductive loop [46]. The Mg(OH)₂ film shows larger R_t and lower C_{dl} than those of bare AZ31 alloy, which indicate less corrosion and better surface protective film integrity. Further, hydrotalcite films demonstrate the higher R_t and lower C_{dl} than Mg(OH)₂ film and shows superior corrosion resistance. Based on the EIS studies, it is observed that hydrothermally treated hydrotalcite films exhibited more corrosion protection in corrosive medium.

Conclusion

The layered double hydroxide based hydrotalcite (Mg₆Al₂CO₃(OH)₁₆·4H₂O) and Mg(OH)₂ films were fabricated on AZ31 alloy by hydrothermal treatment. The XRD results demonstrated that hydrotalcite belongs to rhombohedral phase, while Mg(OH)₂ corresponds to hexagonal phase. The hexagonal Mg(OH)₂ films and rhombohedral hydrotalcite films are also characterized by laser Raman technique, where CO₃²⁻ and OH⁻ groups were identified. The potentiodynamic polarization curves demonstrates more positive corrosion potentials for hydrotalcite and more negative for bare AZ31, while Mg(OH)₂ films

demonstrated intermediate potentials. The corrosion currents also exhibit the same trend. The electrochemical impedance spectroscopy also follows the same trend. The formation of layered double hydroxide of magnesium with carbonates on AZ31 alloy led the more protection and this work paves newer directions on hydrothermal surface modification of magnesium alloys.

CONFLICT OF INTEREST

The authors declare that there is no conflict of interests regarding the publication of this article.

REFERENCES

- B.L. Mordike and T. Ebert, *Mater. Sci. Eng. A*, **302**, 37 (2001); [https://doi.org/10.1016/S0921-5093\(00\)01351-4](https://doi.org/10.1016/S0921-5093(00)01351-4).
- S. Thomas, N.V. Medhekar, G.S. Frankel and N. Birbilis, *Curr. Opin. Solid State Mater. Sci.*, **19**, 85 (2015); <https://doi.org/10.1016/j.cossms.2014.09.005>.
- R. Wu, Y. Yan, G. Wang, L. E. Murr, W. Han, Z. Zhang and M. Zhang, *Int. Mater. Rev.*, **60**, 65 (2015); <https://doi.org/10.1179/1743280414Y.00000000044>.
- L. Hou, T. Wang, R. Wu, J. Zhang, M. Zhang, A. Dong, B. Sun, S. Betsofen and B. Krit, *J. Mater. Sci. Technol.*, **34**, 317 (2018); <https://doi.org/10.1016/j.jmst.2017.02.005>.
- M. Esmaily, D.B. Blücher, R.W. Lindstrom, J.E. Svensson and L.G. Johansson, *J. Electrochem. Soc.*, **162**, C260 (2015); <https://doi.org/10.1149/2.0801506jes>.
- M. Shahabi-Navid, M. Esmaily, J.E. Svensson, M. Halvarsson, L. Nyborg, Y. Cao and L.G. Johansson, *J. Electrochem. Soc.*, **161**, C277 (2014); <https://doi.org/10.1149/2.088405jes>.
- Z. Pu, S. Yang, G.-L. Song, O.W. Dillon Jr., D.A. Puleo and I.S. Jawahir, *Scr. Mater.*, **65**, 520 (2011); <https://doi.org/10.1016/j.scriptamat.2011.06.013>.
- M. Danaie, R.M. Asmussen, P. Jakupi, D.W. Shoesmith and G.A. Botton, *Corros. Sci.*, **77**, 151 (2013); <https://doi.org/10.1016/j.corsci.2013.07.038>.
- R.M. Asmussen, P. Jakupi, M. Danaie, G.A. Botton and D.W. Shoesmith, *Corros. Sci.*, **75**, 114 (2013); <https://doi.org/10.1016/j.corsci.2013.05.022>.
- H.-Y. Ha, H.J. Kim, S.-M. Baek, B. Kim, S.-D. Sohn, H.-J. Shin, H.Y. Jeong, S.H. Park, C.D. Yim, B.S. You, J.G. Lee and S.S. Park, *Scr. Mater.*, **109**, 38 (2015); <https://doi.org/10.1016/j.scriptamat.2015.07.013>.
- R.K. Singh Raman, N. Birbilis and J. Efthimiadis, *Corros. Eng. Sci. Technol.*, **39**, 346 (2004); <https://doi.org/10.1179/174327804X13208>.
- M. Esmaily, M. Shahabi-Navid, J.E. Svensson, M. Halvarsson, L. Nyborg, Y. Cao and L.G. Johansson, *Corros. Sci.*, **90**, 420 (2015); <https://doi.org/10.1016/j.corsci.2014.10.040>.
- J. Liu, Y. Song, J. Chen, P. Chen, D. Shan and E.H. Han, *Electrochim. Acta*, **189**, 190 (2016); <https://doi.org/10.1016/j.electacta.2015.12.075>.
- H. Ardelean, I. Frateur, S. Zanna, A. Atrens and P. Marcus, *Corros. Sci.*, **51**, 3030 (2009); <https://doi.org/10.1016/j.corsci.2009.08.030>.
- L. Chai, X. Yu, Z. Yang, Y. Wang and M. Okido, *Corros. Sci.*, **50**, 3274 (2008); <https://doi.org/10.1016/j.corsci.2008.08.038>.
- F. Pan, X. Yang and D. Zhang, *Appl. Surf. Sci.*, **255**, 8363 (2009); <https://doi.org/10.1016/j.apsusc.2009.05.089>.
- A.J. López, J. Rams and A. Ureña, *Surf. Coat. Technol.*, **205**, 4183 (2011); <https://doi.org/10.1016/j.surfcoat.2011.03.011>.
- C. Taltavull, B. Torres, A.J. Lopez, P. Rodrigo, E. Otero, A. Atrens and J. Rams, *Mater. Des.*, **57**, 40 (2014); <https://doi.org/10.1016/j.matdes.2013.12.069>.
- G. Reiners and M. Griepentrog, *Surf. Coat. Technol.*, **76-77**, 809 (1995); [https://doi.org/10.1016/02578-9729\(50\)26088-](https://doi.org/10.1016/02578-9729(50)26088-).
- G. Wu, W. Dai, H. Zheng and A. Wang, *Surf. Coat. Technol.*, **205**, 2067 (2010); <https://doi.org/10.1016/j.surfcoat.2010.08.103>.

21. L. Zhao and E. Lugscheider, *Surf. Coat. Technol.*, **162**, 6 (2003); [https://doi.org/10.1016/S0257-8972\(02\)00560-1](https://doi.org/10.1016/S0257-8972(02)00560-1).
22. T.F. Kubatík, Z. Pala, K. Neufuss, M. Vilémová, R. Musálek, J. Stoulil, P. Slepíčka and T. Chráska, *Surf. Coat. Technol.*, **282**, 163 (2015); <https://doi.org/10.1016/j.surfcoat.2015.10.032>.
23. J. Formosa, J.M. Chimenos, A.M. Lacasta and L. Haurie, *Thermochim. Acta*, **515**, 43 (2011); <https://doi.org/10.1016/j.tca.2010.12.018>.
24. E. Suzuki, Y. Nomoto, M. Okamoto and Y. Ono, *Catal. Lett.*, **48**, 75 (1997); <https://doi.org/10.1023/A:1019050314878>.
25. R.V. Siriwardane and R.W. Stevens Jr., *Ind. Eng. Chem. Res.*, **48**, 2135 (2009); <https://doi.org/10.1021/ie8011598>.
26. J. Lv, L. Qiu and B. Qu, *J. Cryst. Growth*, **267**, 676 (2004); <https://doi.org/10.1016/j.jcrysgro.2004.04.034>.
27. Y. Ding, G. Zhang, H. Wu, B. Hai, L. Wang and Y. Qian, *Chem. Mater.*, **13**, 435 (2001); <https://doi.org/10.1021/cm000607e>.
28. C. Yan, D. Xue, L. Zou, X. Yan and W. Wang, *J. Cryst. Growth*, **282**, 448 (2005); <https://doi.org/10.1016/j.jcrysgro.2005.05.038>.
29. M. Dinamani and P.V. Kamath, *J. Appl. Electrochem.*, **34**, 899 (2004); <https://doi.org/10.1023/B:JACH.0000040437.81319.56>.
30. Y. Zhu, Q. Zhao, Y.-H. Zhang and G. Wu, *Surf. Coat. Technol.*, **206**, 2961 (2012); <https://doi.org/10.1016/j.surfcoat.2011.12.029>.
31. Y. Zhu, G. Wu, Y.-H. Zhang and Q. Zhao, *Appl. Surf. Sci.*, **257**, 6129 (2011); <https://doi.org/10.1016/j.apsusc.2011.02.017>.
32. T. Ishizaki, S.-P. Cho and N. Saito, *CrystEngComm*, **11**, 2338 (2009); <https://doi.org/10.1039/b907490b>.
33. R. Salomão, L.M. Milena, M.H. Wakamatsu and V.C. Pandolfelli, *Ceram. Int.*, **37**, 3063 (2011); <https://doi.org/10.1016/j.ceramint.2011.05.034>.
34. S. Nishimura, A. Takagaki and K. Ebitani, *Green Chem.*, **15**, 2026 (2013); <https://doi.org/10.1039/c3gc40405f>.
35. A. Vaccari, *Appl. Clay Sci.*, **22**, 75 (2002); [https://doi.org/10.1016/S0169-1317\(02\)00112-6](https://doi.org/10.1016/S0169-1317(02)00112-6).
36. S. Miyata and T. Kumura, *Chem. Lett.*, **2**, 843 (1973); <https://doi.org/10.1246/cl.1973.843>.
37. M. Ogawa and H. Kaiho, *Langmuir*, **18**, 4240 (2002); <https://doi.org/10.1021/la0117045>.
38. Y. Yang, X. Zhao, Y. Zhu and F. Zhang, *Chem. Mater.*, **24**, 81 (2012); <https://doi.org/10.1021/cm201936b>.
39. Z.P. Xu, G.S. Stevenson, C.Q. Lu, G.Q. Lu, P.F. Bartlett and P.P. Gray, *J. Am. Chem. Soc.*, **128**, 36 (2006); <https://doi.org/10.1021/ja056652a>.
40. Q. Wang, H.H. Tay, Z. Guo, L. Chen, Y. Liu, J. Chang, Z. Zhong, J. Luo and A. Borgna, *Appl. Clay Sci.*, **55**, 18 (2012); <https://doi.org/10.1016/j.clay.2011.07.024>.
41. F. Winter, A.J. van Dillen and K.P. de Jong, *Chem. Commun.*, 3977 (2005); <https://doi.org/10.1039/b506173c>.
42. S. Miyata, *Clays Clay Miner.*, **31**, 305 (1983); <https://doi.org/10.1346/CCMN.1983.0310409>.
43. D. Song, A.B. Ma, J. Jiang, P. Lin, D. Yang and J. Fan, *Corros. Sci.*, **52**, 481 (2010); <https://doi.org/10.1016/j.corsci.2009.10.004>.
44. C. Yao, H. Lv, T. Zhu, W. Zheng, X. Yuan and W. Gao, *J. Alloys Compd.*, **670**, 239 (2016); <https://doi.org/10.1016/j.jallcom.2016.02.026>.
45. M. Mosialek, G. Mordarski, P. Nowak, W. Simka, G. Nawrat, M. Hanke, R.P. Socha and J. Michalska, *Surf. Coat. Technol.*, **206**, 51 (2011); <https://doi.org/10.1016/j.surfcoat.2011.06.035>.
46. M. Razavi, M. Fathi, O. Savabi, D. Vashae and L. Tayebi, *Mater. Sci. Eng. C*, **41**, 168 (2014); <https://doi.org/10.1016/j.msec.2014.04.039>.